IOP PUBLISHING PHYSICS IN MEDICINE AND BIOLOGY

Phys. Med. Biol. **54** (2009) 1253–1264 doi:10.1088/0031-9155/54/5/010

Ultra fast electromagnetic field computations for RF multi-transmit techniques in high field MRI

Bob van den Bergen[1], Christiaan C Stolk[2], Jan Bouwe van den Berg[3], Jan J W Lagendijk[1] and Cornelis A T Van den Berg[1]

[1] Department of Radiotherapy, University Medical Center Utrecht, PO Box 85500, HP Q.00.118, 3508 GA, Utrecht, The Netherlands
[2] Department of Applied Mathematics, University of Twente, PO Box 217, 7500 AE, Enschede, The Netherlands
[3] Department of Mathematics, VU University Amsterdam, De Boelelaan 1081, 1081 HV, Amsterdam, The Netherlands

E-mail: B.vandenBergen@UMCUtrecht.nl

Received 1 July 2008, in final form 9 December 2008
Published 30 January 2009
Online at stacks.iop.org/PMB/54/1253

Abstract

A new, very fast, approach for calculations of the electromagnetic excitation field for MRI is presented. The calculation domain is divided in different homogeneous regions, where for each region a general solution is obtained by a summation of suitable basis functions. A unique solution for the electromagnetic field is found by enforcing the appropriate boundary conditions between the different regions. The method combines the speed of an analytical method with the versatility of full wave simulation methods and is validated in the pelvic region against FDTD simulations at 3 and 7 T and measurements at 3 T. The high speed and accurate reproduction of measurements and FDTD calculations are believed to offer large possibilities for multi-transmit applications, where it can be used for on-line control of the global and local electric field and specific absorption rate (SAR) in the patient. As an example the method was evaluated for RF shimming with the use of 7 T simulation results, where it was demonstrated that the magnetic excitation field could be homogenized, while both the local and average SAR were reduced by 38% or more.

(Some figures in this article are in colour only in the electronic version)

1. Introduction

The increase in magnetic field strength for magnetic resonance imaging over the last decade has introduced new challenges related to the radiofrequency (RF) transmit field. The RF excitation field has become much more heterogeneous (Collins *et al* 2005, Liu *et al* 2005,

Vaughan *et al* 2001) and also the energy deposition in the patient, which is measured as specific absorption rate (SAR), has considerably increased (Collins and Smith 2001, Ibrahim and Tang 2007).

Parallel excitation (Katscher *et al* 2003) and RF shimming (Collins *et al* 2007, Ibrahim 2006, Van den Berg *et al* 2007a, Van den Bergen *et al* 2007) have been proposed as methods for coping with these RF issues. However, both methods require information about the RF fields that are created by the individual antenna elements around the patient before they can be applied to change the characteristics of the total field. It was already proposed to use generic, patient independent, electromagnetic fields for RF shimming (Van den Berg *et al* 2007a, Van den Bergen *et al* 2007), but although satisfying results were obtained, the lack of patient specific fields can only result in suboptimal solutions. Measurements have been successfully used to provide patient specific information about the magnetic part $\left(B_1^+\right)$ of the RF field for RF shimming (Metzger *et al* 2008), but measurements cannot provide similar information about the electric part of the RF field. It is this electric part that is responsible for energy deposition in the patient, which results in tissue heating and thereby causes a serious safety concern for ultra high-field MRI. Successful implementation of either parallel excitation or RF shimming in a practical setting can only be achieved when this local energy deposition can be monitored and preferably also controlled.

Calculations, contrary to measurements, do provide a means to obtain both the electric and magnetic part of the RF field, but they also have some disadvantages. Full wave simulation methods such as the finite difference time domain method (FDTD) (Ibrahim *et al* 2000) and the method of moments (Jin *et al* 1996), for example, have shown excellent agreement with measurements and have been very successful for research purposes. Unfortunately simulations like these are much too slow for real time use in a clinical setting. Analytical solutions on the other hand provide very fast field calculations, but are only applicable for a small set of homogeneous geometries such as cylinders, ellipses and spheres (Bottomley and Andrew 1978, Bottomley *et al* 1985, Hoult and Phil 2000, Sled and Pike 1998, Glover *et al* 1985). These geometries show little resemblance to real anatomical structures and are therefore also primarily used for research purposes.

In this study we will use a new approach for electromagnetic field calculations (Van den Berg *et al* 2007b), which we validate in the pelvic region and test for its use in RF shimming. The method combines the speed of an analytical method with the versatility of full wave simulation methods. Variable geometry shapes can be used and also the positions and the number of antenna elements can be arbitrary chosen. The method continues on the basic principles of the analytical method provided by Foo *et al* (1991), which was extended by Spence and Wright (Spence and Wright 2003). Like Foo *et al* we divide the domain into different regions and we use a set of basis functions for the solutions on each domain obtained by separation of variables in cylindrical coordinates, i.e. Bessel functions. However, we do not use a cylindrical geometry for the patient like Foo *et al* but we use real patient contours, which makes it impossible to obtain an analytic solution. Instead, we calculate the suitable Bessel coefficients for each region to enforce the boundary conditions on the patient contour. The method shall be referred to as Bessel boundary matching (BBM).

The speed and versatility of the BBM method are believed to offer large possibilities for multi-transmit applications such as RF shimming and parallel excitation, where on-line calculations of the magnetic field can be used to confirm or maybe even replace magnetic field measurements. The biggest advantage however comes from the ability to calculate simultaneously the electric fields in the patient. This provides a method for on-line reduction of both the average and local SAR.

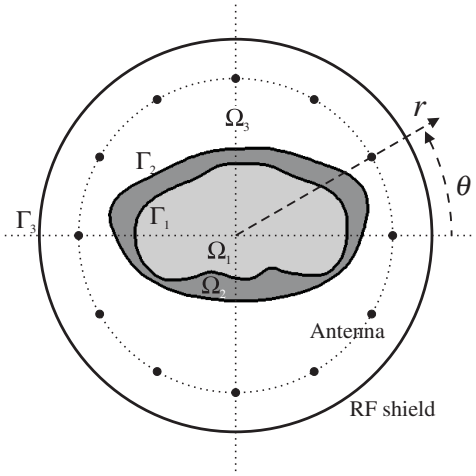

Figure 1. A two-dimensional model of the inside of a conventional MRI scanner that forms the calculation domain. Various regions (Ω_1 , Ω_2 and Ω_3) and boundaries (Γ_1, Γ_2 and Γ_3) are identified.

2. Theory

The problem is described in cylindrical coordinates, which naturally fit the geometry of a conventional MRI scanner. The RF electromagnetic field inside the MRI scanner is calculated under the assumption that the problem is two-dimensional, which implies that the spatial derivative of the electromagnetic field in the longitudinal (z) direction is zero. Previous reports (Van den Berg *et al* 2007a, Van den Bergen *et al* 2007) have shown that this assumption is reasonable for body imaging in the central region of a body coil. A review of the simulations performed for these studies showed less than 5% variation in the z-component of the electric field over a length of 15 and 10 cm around the central plane in the longitudinal direction at 3 T and 7 T respectively for a homogeneous phantom. However, these numbers are coil dependent and since we only used very simple centre-fed dipole elements (32 cm at 7 T, 58 cm at 3 T) without, for instance, distributed capacitors to enhance current homogeneity over the coil elements, this is likely to be a conservative estimate for commercially available TEM coils.

The two-dimensional calculation domain is shown in figure 1. The BBM method requires every region in this domain to have a homogeneous electric permittivity and conductivity. For theoretical purposes we have chosen to identify three regions, which all have a different type of solution. A distinction between the air Ω_1 and the body is obvious. The body is further segmented in an outer fat layer (Ω_2) and an inner layer consisting of muscle, bone and various organs (Ω_3), but also other or more segmentations are possible.

The antenna elements of the RF coil are included in the outer region as ideal line sources. We have defined their position equidistantly on a ring around the origin for simplicity, but this is not a prerequisite. The position and also the number of elements can be arbitrarily chosen.

The behaviour of the electromagnetic fields in the MRI scanner is described by the Maxwell equations in non-dispersive isotropic media. These equations can be simplified by the introduction of the vector potential $\mathbf{A}$ and the scalar potential and by the use of the gauge freedom to eliminate the latter. With these simplifications a single Helmholtz equation (1) for the vector potential can be obtained from the Maxwell equations, see e.g. Griffiths (1999),

with ϵ and μ being the dielectric and magnetic permeability, respectively and $\mathbf{J}$ is the free current

$$\epsilon\mu\frac{\partial^2\mathbf{A}}{\partial t^2} = \nabla^2\mathbf{A} + \mu\mathbf{J}. \tag{1}$$

The free current $\mathbf{J}$ in the Helmholtz equation (1) can be separated into the induced currents ($\mathbf{J}_{\text{ind}}$) and the external currents ($\mathbf{J}_{\text{ext}}$). The induced currents are a simple function of the vector potential, the frequency (ω) and the electric conductivity (σ), when we assume that all fields oscillate harmonically with the same frequency as the sources

$$\mathbf{J}_{\text{ind}} = \sigma\mathbf{E} = -\sigma\frac{\partial\mathbf{A}}{\partial t} = -\mathrm{i}\omega\sigma\mathbf{A}. \tag{2}$$

The external currents are the currents running through the antenna elements along the z-dimension, which in two dimensions are modelled as delta peaks at the locations of the antennas. The contribution of all antenna elements is a simple summation of the individual contributions of all (N) elements

$$\mathbf{J}_{\text{ext}} = \sum_{l=1}^{N} I_l\,\mathrm{e}^{\mathrm{i}\omega t}\delta(r - r_l)\delta(\theta - \theta_l)\hat{z}, \tag{3}$$

where I_l is the complex amplitude and (r_l, θ_l) is the position of the lth antenna element.

We now assume that the transverse components of the electric field and the vector potential can be neglected, which is based on the observation that for body imaging the component of the electric field along the longitudinal (z) direction is roughly an order of magnitude larger than its transverse components (Van den Berg *et al* 2007a, Van den Bergen *et al* 2007). These assumptions allow further simplification of equation (1):

$$\xi^2 A_z + \nabla^2 A_z = -\mu\mathbf{J}_{\text{ext}}, \tag{4}$$

with $\xi^2 = \epsilon\mu\omega^2 - \mathrm{i}\omega\sigma\mu$.

The boundary conditions for the vector potential can be derived from the general electromagnetic boundary conditions for the electric and magnetic field. The continuity of the parallel component of the electric field translates to the continuity of A_z throughout the calculation domain. The continuity of the magnetic field requires that the curl of $\mathbf{A}$ must be continuous, which translates to the continuity of the spatial derivative of the vector potential. The outer boundary of the calculation domain is formed by the metallic RF shield, where A_z is assumed to be zero due to the high conductivity of the metal.

We will now recast the simplified Helmholtz equation (4) to describe the fields in the geometry of figure 1 for a single antenna element. The total field is thereafter calculated as the complex summation of the individual fields. Both ξ and $\mathbf{J}_{\text{ext}}$ are region dependent and therefore the Helmholtz equation needs to be solved for each region individually. The solutions for the different regions can be joined together by imposing the boundary conditions. There are no external currents in regions Ω_1 and Ω_2, which means that the inhomogeneous Helmholtz equation turns into a homogeneous one

$$\xi^2 A_z + \nabla^2 A_z = 0. \tag{5}$$

The solution to equation (5) is obtained with separation of variables in cylindrical coordinates. A general solution is an infinite summation of first (J) and second (Y) kind radial Bessel functions, which are multiplied with angular complex exponentials. It should be noted that the second kind radial Bessel functions give a pole in the origin, which is physically impossible for region Ω_1. Therefore, for region Ω_1 the general solution is simplified. a and b

are the Bessel coefficients for the first and second kind radial Bessel functions, respectively

$$A_{z,\Omega_1} = \sum_{m=-\infty}^{\infty} a_{1,m} J_m(\xi_1 r)\, \mathrm{e}^{\mathrm{i}m\theta} \tag{6a}$$

$$A_{z,\Omega_1} \equiv a_1 \Phi_1, \tag{6b}$$

$$A_{z,\Omega_2} = \sum_{m=-\infty}^{\infty} a_{2,m} J_m(\xi_2 r)\, \mathrm{e}^{\mathrm{i}m\theta} + \sum_{n=-\infty}^{\infty} b_{2,n} Y_n(\xi_2 r)\, \mathrm{e}^{\mathrm{i}n\theta} \tag{7a}$$

$$A_{z,\Omega_2} \equiv a_2 \Phi_2 + b_2 \Psi_2. \tag{7b}$$

The antenna elements in region Ω_3 provide external currents, which means that the inhomogeneous Helmholtz equation must be solved in this region

$$\xi^2 A_z + \nabla^2 A_z = -\mu \sum_{l=1}^{N} I_l\, \mathrm{e}^{\mathrm{i}\omega t} \delta(r - r_l)\delta(\theta - \theta_l)\hat{z}. \tag{8}$$

The general solution to the inhomogeneous Helmholtz equation (8) is obtained by adding a fundamental solution (F_l) to the solution of the homogeneous Helmholtz equation, which is a solution to the equation

$$\xi_3^2 F_l + \nabla^2 F_l = -\delta(r - r_l)\delta(\theta - \theta_l)\hat{z}, \tag{9}$$

where (r_l, θ_l) is the position of the lth antenna. A fundamental solution is readily given by

$$F_l = -\tfrac{1}{4} Y_0(\xi_3 \rho_l), \tag{10}$$

where $\rho_l(r, \theta) = r^2 + r_l^2 - 2 r r_l \cos(\theta - \theta_l)$ is the distance from the antenna. The complete solution to the inhomogeneous Helmholtz equation in Ω_3 is then given by

$$A_{z,\Omega_3} = -\frac{1}{4} Y_0(\xi_3 \rho_l) + \sum_{m=-\infty}^{\infty} a_{3,m} J_m(\xi_3 r)\, \mathrm{e}^{\mathrm{i}m\theta} + \sum_{n=-\infty}^{\infty} b_{3,n} Y_n(\xi_3 r)\, \mathrm{e}^{\mathrm{i}n\theta} \tag{11a}$$

$$A_{z,\Omega_3} \equiv F + a_3 \Phi_3 + b_3 \Psi_3. \tag{11b}$$

The general solutions for all regions can be cast into a unique solution by the calculation of the Bessel coefficients a and b that enforce the continuity of A_z and its spatial derivative throughout the calculation domain. Using the shorter notation introduced in equations (6b), (7b) and (11b) the boundary equations can be combined into a single matrix equation

$$\begin{bmatrix} \Phi_1|_{\Gamma_1} & -\Phi_2|_{\Gamma_1} & -\Psi_2|_{\Gamma_1} & 0 & 0 \\ \frac{\partial \Phi_1}{\partial n}|_{\Gamma_1} & -\frac{\partial \Phi_2}{\partial n}|_{\Gamma_1} & -\frac{\partial \Psi_2}{\partial n}|_{\Gamma_1} & 0 & 0 \\ 0 & \Phi_2|_{\Gamma_2} & \Psi_2|_{\Gamma_2} & -\Phi_3|_{\Gamma_2} & -\Psi_3|_{\Gamma_2} \\ 0 & \frac{\partial \Phi_2}{\partial n}|_{\Gamma_2} & \frac{\partial \Psi_2}{\partial n}|_{\Gamma_2} & -\frac{\partial \Phi_3}{\partial n}|_{\Gamma_2} & -\frac{\partial \Psi_3}{\partial n}|_{\Gamma_2} \\ 0 & 0 & 0 & \Phi_3|_{\Gamma_3} & \Psi_3|_{\Gamma_3} \end{bmatrix} \begin{bmatrix} a_1 \\ a_2 \\ b_2 \\ a_3 \\ b_3 \end{bmatrix} = \begin{bmatrix} 0 \\ 0 \\ F|_{\Gamma_2} \\ \frac{\partial F}{\partial n}|_{\Gamma_2} \\ -F|_{\Gamma_3} \end{bmatrix}. \tag{12}$$

This matrix can be solved for the Bessel coefficients when the boundaries are discretized and when a finite number of Bessel modes is taken into account. With these coefficients the

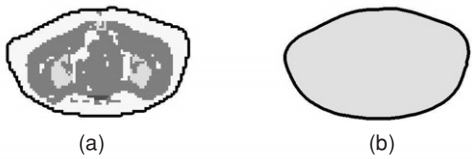

Figure 2. Difference between the female anatomy model for the FDTD method that has been segmented in (from light to dark) fat, bone, muscle and air (a) and the female anatomy model for the BBM method (b). Note that the contour of the BBM model is based on the contour of the FDTD model, but that the boundary has been smoothed to remove any staircasing that hampers the matching at the boundary.

complete solution for the vector potential can be obtained, which allows the calculation of the electric field and the magnetic excitation field $\left(B_1^+\right)$.

3. Methods

Although the BBM method allows for multiple different regions, we only used a single region with a fixed electric conductivity and permittivity to describe the patients and ellipses for the BBM method. Segmentation of the outer fat layer was tested for the patient anatomies, but this made the boundary matching procedure more cumbersome in certain situations (see discussion), while no improvements in the calculated fields were observed.

Two different ellipses and a CT-based female anatomy model were used to validate the BBM method against three-dimensional FDTD calculations. The ellipses were completely homogeneous and therefore identical for both methods. However, the female anatomy was segmented based on Hounsfield thresholding (Van de Kamer *et al* 2001), with tissue parameters obtained from http://www.fcc.gov/cgi-bin/dielec.sh. This segmentation could only be used for the FDTD calculations and not for the BBM calculations where it was replaced by the average dielectric properties of the female anatomy model to obtain a single homogeneous region (figure 2).

Next to the FDTD simulations we also compared the BBM calculations with B_1^+ measurements of two patients. The anatomy contour of these patients was manually delineated in a survey image, after which it was used as an input for the BBM method. The electric conductivity and permittivity were chosen equal to the weighted average of the segmented female anatomy used for the FDTD simulations. The measurements were made on a Philips 3 Tesla Achieva scanner, using the standard available pulsed steady state sequence (Yarnykh 2007).

The matrix equation (12) was implemented in Matlab® and solved for all Bessel coefficients. The boundary matching was done in the Fourier domain, which allowed the transformation of the matrix from an overdetermined system into a square matrix by taking only as many Fourier components into account as there were Bessel modes. Alternatively, it is also possible to solve the overdetermined system using a least-squares inversion. The calculation domain was discretized in 150 × 150 pixels, which resulted in a resolution of approximately 4.5 mm. Each boundary was described by 1024 points, which were distributed with equal azimuthal angles. One hundred and twenty five Bessel modes were taken into account, both for the first and second kind. The electric and magnetic field were calculated and matched at the boundaries individually for each antenna, after which the total field was calculated as a complex superposition of the individual fields. This allowed easy RF shimming

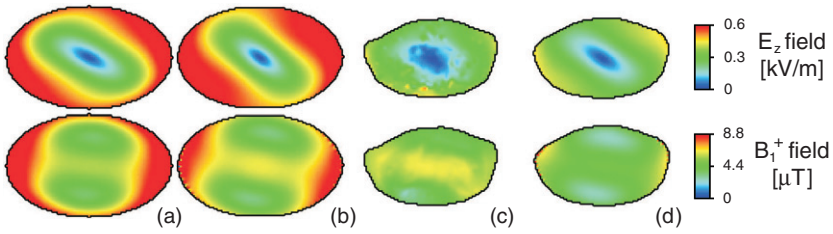

Figure 3. Comparison between FDTD and BBM at 3 T for quadrature settings. (a) Homogeneous ellipse, FDTD. (b) Homogeneous ellipse, BBM. (c) Segmented patient, FDTD. (d) Homogeneous patient, BBM.

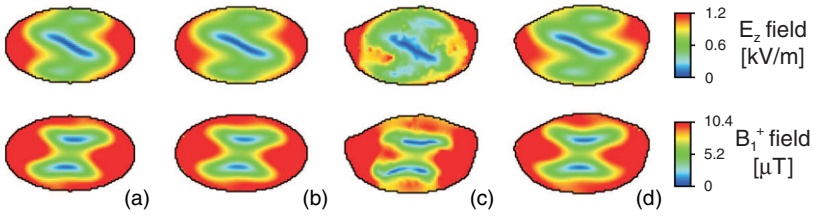

Figure 4. Comparison between FDTD and BBM at 7 T for quadrature settings. (a) Homogeneous ellipse, FDTD. (b) Homogeneous ellipse, BBM. (c) Segmented patient, FDTD. (d) Homogeneous patient, BBM.

because the individual fields only needed to be calculated once and only the last step, where the fields are added together, had to be repeated for new phase amplitude settings.

To demonstrate the potential of the BBM method for multi-transmit purposes, we have tested its use for RF shimming. A nonlinear constrained optimization was used, where the phases and amplitudes of the individual antenna elements were optimized to make the standard deviation of the B_1^+ field as small as possible in a central disk with a diameter of 7 cm, while the average B_1^+ in this disk was normalized to an average flip angle of 90°. The constraint was used to enforce the quotient of the maximum and average electric field to stay below a certain constant to reduce the maxima in the electric field. Since the SAR scales quadratically with the electric field, this is a simple method to reduce both the average SAR and the local SAR peaks. It must be stressed that this constraint is very basic and is only used as a 'proof of principle' to show the potential for SAR reduction with the BBM method rather than to demonstrate its full potential.

4. Results

The calculation time for the total electric and magnetic fields resulting from 12 antenna elements was 24 ± 3 s for each anatomy on a standard desktop computer with an Intel® Pentium® 4, 3.40 GHz processor. This time included ∼7 s for initializing the problem and solving the matrix for the Bessel coefficients for all 12 antennas, ∼10 s to identify for each point in the calculation domain to which region it belonged and ∼7 s for the summation of all Bessel modes to obtain the total fields.

We first compared the results of the BBM method with standard FDTD simulations at 128 MHz (3 T) and at 300 MHz (7 T) both for an ellipse and for a real anatomy. At 3 T (figure 3) and at 7 T (figure 4) the results show a very strong resemblance with FDTD

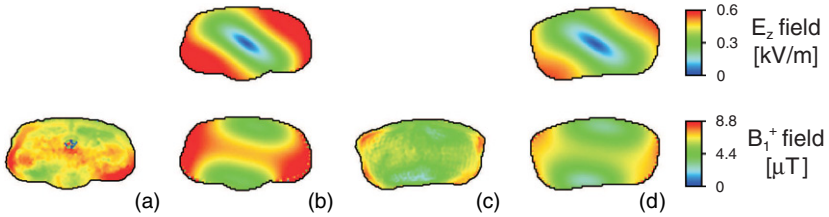

Figure 5. Comparison between measurements and BBM at 3 T for quadrature settings. (a) Real patient, measurement. (b) Homogeneous patient, BBM. (c) Real patient, measurement. (d) Homogeneous patient, BBM.

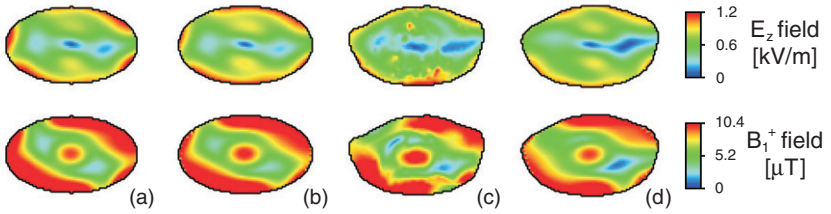

Figure 6. Comparison between FDTD and BBM results at 7 T for RF shimming. (a) Homogeneous ellipse, FDTD. (b) Homogeneous ellipse, BBM. (c) Segmented patient, FDTD. (d) Homogeneous patient, BBM.

simulations for the electric and magnetic field. For the real anatomy this resemblance is locally somewhat diminished by tissue variations that are only present in the FDTD model and not in the model used for the BBM method. At 3 T their influence looks somewhat more pronounced than at 7 T.

The next step was comparing the BBM calculations with B_1^+ maps that were taken from our patient database. These measurements show some larger local variations than the FDTD simulations, but there is still a good correspondence between the measurements and the calculations with the BBM method (figure 5). Note some minor repetitive errors at the edges in the B_1^+ field, which can be attributed to some residual error in the fitting process. The nominal flip angle of the measurements was scaled to match the scale of the BBM method.

The results of RF shimming with the BBM method are shown in figure 6. After calculation of the individual antenna fields, the resulting total B_1^+ field in the central region of the ellipse and female anatomy were individually homogenized while the quotient of the maximum and average electric field was constrained. This optimization took 2–3 min dependent on the value of the constraint. The optimized phase amplitude settings were thereafter also used for the fields that were calculated with the FDTD method, which resulted in very comparable field patterns (figure 6). Moreover, because the FDTD calculations included a full three-dimensional model, it was possible to evaluate the average and maximum SAR in the entire anatomy rather than in a single slice. The phase amplitude settings that were calculated based on the BBM fields resulted in a reduction of the average SAR (for a 90° gradient echo sequence with a pulse length of 1 ms and a repetition time of 20 ms) in the full 60 cm high model from 4.8 to 2.9 W kg^{-1} (−40%) for the ellipse and from 3.2 to 2.0 W kg^{-1} (−38%) for the female anatomy. The local maximum SAR in any 5 mm cubic voxel reduced from 34.5 to 20.9 W kg^{-1} (−39%) for the ellipse and from 74.0 to 37.6 W kg^{-1} (−49%) for the female anatomy.

5. Discussion

The presented BBM method has shown to be able to reproduce FDTD calculations and measurements very well. The ellipses, which were homogeneous both for the BBM and for the FDTD calculations, showed excellent agreement (figures 3(a), (b) and 4(a), (b)) and only small local deviations were visible for the segmented female anatomy and for the measurements. These can be attributed to the fact that the BBM method cannot resolve the local tissue related variations due to the absence of an internal dielectric structure.

Some of the calculations show a repetitive pattern along the boundaries in the magnetic field. This can be attributed to a small residual error in the boundary matching. Tuning of the number of boundary points and the number of Bessel functions can reduce these errors, but we choose to use a single setting for all calculations, which on average gave the best result. This was done because it is expected that in a practical setting it is unfeasible to tune these numbers on a patient specific basis. However, it might be possible to develop an algorithm that estimates the required number of modes and boundary points based on some automatically established boundary characteristics such as ellipticity and smoothness. These errors at the boundary are only visible in the magnetic field and not in the electric field, because the curl operation that is performed to obtain the magnetic field tends to amplify any errors in the vector potential field.

Possible limitations for the BBM method result from the assumptions that have been made. In the pelvic region these are easily defended and validated by the shown results, but for other regions in the body they need to be investigated. For instance the assumption that the transverse components of the electric field can be neglected in favour of the longitudinal component might only be valid in certain parts of the body. Also the requirement that the derivative of the electric field in the longitudinal direction is close to zero is region dependent and will not hold in regions where the body shape varies significantly as is for instance the case at the junctions between the torso and the limbs. A further limitation might be related to the type of coil geometry that is used as some coils might create local SAR peaks around the extremities of the coil. However, these SAR peaks were not observed in our FDTD simulations.

Another possible issue is the fact that the currents on the antennas are assumed to be independent of the load and antenna coupling. Again, for the calculations that were done this was shown not to be a problem, but it might become important for coil design applications when for instance surface coils are compared to volume coils or when strip line elements are compared to loop elements.

The BBM method is very versatile. Both the number of regions and the number of antenna elements can be arbitrarily chosen. Thirty-six antenna elements were successfully tested as well as three different regions, where the patient was segmented in an outer fat layer and an inner region of muscle, bone and organs. However, when the outer fat layer was locally very thin (e.g. figure 2(a), bottom left and right corner) this segmentation of the patient hampered fitting of the boundary conditions, resulting in local errors. This is not inherent to the method but more a consequence of the chosen resolution and basis functions. Other types of basis functions and possibly a shift of their origin as well as an increased resolution might improve the boundary matching. Besides the computational difficulties no significant differences were observed between calculations with and without the segmentation of the outer fat layer, which in itself is already quite a remarkable result. This segmentation was therefore discarded and the patient was only modelled as a single homogeneous region. No further efforts were made to improve the boundary matching in the presence of such a locally thin fat layer. However, for other regions in the body or for very obese patients, where this fat layer is everywhere sufficiently thick, this extra segmentation might prove useful.

The use of Matlab® allowed easy implementation of the method, but it is known to be a relatively slow computation platform. The average computation time of 24 s for the complete electric and magnetic field could be reduced by implementing the method in a more 'low level' programming language. Other factors that influence the calculation speed are the number of boundary points, the number of Bessel functions, the number of antenna elements and the number of regions in which the body is segmented. The influence of the first two is limited, but especially the number of regions plays an important role. We used a single region to describe the patient geometry but when an extra region was tested, the calculation time increased from 24 to roughly 70 s.

For the application of the BBM method in a clinical setting we envision a system where the patient contour in the scanner is automatically determined based on a survey image, after which it is used as an input for the BBM method. The average tissue conductivity and permittivity for the model can be based on a predetermined average value. We used the same average values for the homogeneous model of the segmented female anatomy and for the model of the two measurements, which gave satisfying results. Changes up to 10% in these values did not result in noticeable differences, thereby indicating that the exact choice of these values is not critical for the results. Alternatively, it might be possible to use a database of different values for patients with different sexes and, for instance, different body mass indices (BMI).

After computation of the fields with the BBM method they can be used for RF shimming or parallel transmission. The calculated magnetic fields can be used to validate or possibly even replace B_1^+ measurements of the individual antennas and the calculated electric fields can be used to control the resulting electric field. A full SAR assessment is difficult due to the fact that the electric field is only obtained in a single slice through the patient, whilst SAR peaks might also occur in other slices. However, the information about the electric field in this single slice can be used to avoid global regions of constructive interference of the electric field. When these regions are removed in this single slice, effectively they are removed from much more slices due to their global nature. This not only leads to a reduction of the average SAR, but also to a reduction of the local SAR peaks since for 7 T body imaging these peaks are most often found in regions with a high global electric field (Van den Bergen *et al* 2007).

To test the feasibility of this approach we have simulated the above scenario. First the individual two-dimensional fields of all antenna elements were calculated with the BBM method. Thereafter, the phase and amplitude settings for these fields were optimized with a simple constrained optimization which homogenized the B_1^+ excitation field in the central region of the model. The constraint was used to limit the ratio between the maximum value and the average value of the resulting electric field. This turned out to be a simple and effective method to limit the SAR due to the quadratic dependence of the SAR on the electric field. More sophisticated constraints might provide better results, but their development is beyond the scope of this paper.

After the optimized settings were calculated, they were applied to the fields that were calculated with FDTD. The resulting fields in the central slice of the model are not only very similar to the BBM fields (figure 6), but also a large reduction of both the peak SAR and the average SAR was obtained. Note that these SAR reductions are evaluated in the complete three-dimensional models that were used for the FDTD simulations. This illustrates the potential of the BBM method for on-line SAR reduction in ultra high field MRI. By reducing the peaks in the electric field in the central slice both the average and peak SAR in the entire three-dimensional model can be reduced by 38% or more.

The BBM method can only calculate the global field behaviour and not the local field disturbances due to an inherent lack of knowledge about the local dielectric structure of the patient. Consequently, only global field behaviour can be corrected with RF shimming, which

means that the success of the method largely depends on the relative strength of the global field pattern with respect to the local, anatomy related, field disturbances. At ultra high field strengths these global variations in the field dominate over locally induced field changes, which makes the method therefore very successful at 7 T.

The BBM method is not only believed to be valuable for multi-transmit purposes, but we also plan to use the method for coil design applications, where parameters such as SNR, excitation field homogeneity and power dissipation are easily calculated as a function of the number of antennas and their positions. The speed of the BBM method allows real optimization of the coil design rather than a trial-and-error approach.

Another important topic will be the application and possible adaptation of the BBM method for other locations in the body. The method is in general applicable and the basis functions are not necessarily Bessel functions. Also the method is not two-dimensional per-se. We plan to extend the method to three dimensions with a multi-two-dimensional approach or preferably with real three-dimensional regions. A likely region for this is the head, where it might be possible to use spherical Bessel functions and spherical harmonics to calculate the fields in an accurate three-dimensional model. A rigorous mathematical derivation for the expansion of the RF field in spherical Bessel harmonics in a spherical phantom has been provided by Hoult and Phil (2000), which might be extendable to allow for arbitrary boundary shapes on which the boundary conditions can be enforced with the method described in this study. However, this will involve extensive mathematical work as not only the functions, but also the requirements for the vector potential will change.

A third topic will be the application of this method for local SAR reduction in parallel excitation. Also the use of this method for RF shimming that has already been demonstrated in this paper will be explored in depth.

6. Conclusions

We have tested a new method for very fast electromagnetic RF field calculations, which gave very satisfying results. Its speed and accurate reproduction of FDTD simulations and measurements in the pelvic region show that this method has potential for multi-transmit methods such as RF shimming and parallel excitation. It does not only allow very fast steering of the magnetic field, but also provides information about the electric field. As an example it was shown that this information can be used for RF shimming to improve the homogeneity of the magnetic field and simultaneously to lower the electric field and thereby reduce the global and implicitly also the local SAR.

The patient contour is accurately modelled in the BBM method, but a possible limitation of the method is the fact that the inside of the patient is modelled as one or possibly two homogeneous regions. As such it cannot replace full wave simulations such as FDTD or measurements of the excitation field. However, for RF shimming and parallel excitation at ultra high field local tissue dependent phenomena are less important than more global field behaviour such as constructive and destructive interference and penetration effects, which are both accurately calculated by the BBM method.

Acknowledgments

We would like to thank all people that collaborated on this project during the ‘Studygroup mathematics and industry 2007’ for their enthusiasm and contributions.

References

Bottomley P A and Andrew E R 1978 RF magnetic field penetration, phase shift and power dissipation in biological tissue: implications for NMR imaging *Phys. Med. Biol.* **23** 630–43

Bottomley P A, Redington R W, Edelstein W A and Schenck J F 1985 Estimating radiofrequency power deposition in body NMR imaging *Magn. Reson. Med.* **2** 336–49

Collins C M, Liu W, Schreiber W, Yang Q X and Smith M B 2005 Central brightening due to constructive interference with, without, and despite dielectric resonance *J. Magn. Reson. Imag.* **21** 192–6

Collins C M and Smith M B 2001 Calculation of B_1 distribution, SNR and SAR for a surface coil adjacent to an anatomically-accurate human body model *Magn. Reson. Med.* **45** 692–9

Collins C M, Wang Z, Mao W, Fang J, Liu W and Smith M B 2007 Array-optimized composite pulse for excellent whole-brain homogeneity in high-field MRI *Magn. Reson. Med.* **57** 470–4

Foo T K F, Hayes C E and Kang Y W 1991 An analytical model for the design of RF resonators for MR body imaging *Magn. Reson. Med.* **21** 165–77

Glover G H, Hayes C E, Pelc N J, Edelstein W A, Mueller O M, Hart H R, Hardy C J, O'Donnell M and Barber W D 1985 Comparison of linear and circular polarization for magnetic resonance imaging *J. Magn. Reson.* **64** 255–70

Griffiths D J 1999 *Introduction to Electrodynamics* (Upper Saddle River, NJ: Prentice-Hall)

Hoult D I and Phil D 2000 Sensitivity and power deposition in a high field imaging experiment *J. Magn. Reson. Imag.* **12** 46–67

Ibrahim T S 2006 Ultrahigh-field MRI whole-slice and localized RF field excitations using the same RF transmit array *IEEE Trans. Med. Imag.* **25** 1341–7

Ibrahim T S, Lee R, Baertlein B A, Kangarlu A and Robitaille P L 2000 Application of finite difference time domain method for the design of birdcage RF head coils using multi-port excitations *Magn. Res. Imag.* **18** 733–42

Ibrahim T S and Tang L 2007 Insight into RF power requirements and B_1 field homogeneity for human MRI via rigorous FDTD approach *J. Magn. Reson. Imag.* **25** 1235–47

Jin J M, Chen J, Chen W C, Gan H, Magin R L and Dimbylow P J 1996 Computation of electromagnetic fields for high-frequency magnetic resonance imaging applications *Phys. Med. Biol.* **41** 2719–38

Katscher U, Boernert P, Leussler C and Van den Brink J S 2003 Transmit SENSE *Magn. Reson. Med.* **49** 144–50

Katscher U, Hanft M, Vernickel P and Findeklee C 2006 Experimental verification of electric properties tomography (ept) *Proc. of 14th Conf. of International Society of Magnetic Resonance in Medicine*

Liu W, Collins C M and Smith M B 2005 Calculations of B_1 distribution, specific energy absorption rate, and intrinsic signal-to-noise ratio for a body-size birdcage coil loaded with different human subjects at 64 and 128 MHz *Appl. Magn. Reson.* **29** 5–18

Metzger G J, Snyder C, Akgun C, Vaughan T, Ugurbil K and Van de Moortele P F 2008 Local B_1^+ shimming for prostate imaging with transceiver arrays at 7 T based on subject-dependent transmit phase measurements *Magn. Reson. Med.* **59** 396–409

Sled J G and Pike G B 1998 Standing-wave and RF penetration artefacts caused by elliptical geometry: an electrodynamic analysis of MRI *IEEE Trans. Med. Imag.* **17** 653–62

Spence D K and Wright S M 2003 2 D full wave solution for the analysis and design of birdcage coils *Concepts Magn. Reson.* B **18b** 15–23

Van de Kamer J B, De Leeuw A A C, Hornsleth S N, Kroeze H, Kotte A N T J and Lagendijk J J W 2001 Development of a regional hyperthermia treatment planning system *Int. J. Hyperthermia* **17** 207–20

Van den Berg C A T, Van den Bergen B, Van de Kamer J B, Raaymakers B W, Bartels L and Lagendijk J J W 2007a Simultaneous B_1^+ homogenization and specific absorption rate hotspot suppression using a magnetic resonance phased array transmit coil *Magn. Reson. Med.* **57** 577–86

Van den Berg J B *et al* 2007b Understanding the electromagnetic field in an MRI scanner *Proc. of the Study Group Mathematics with Industry 2007*

Van den Bergen B, Van den Berg C A T, Bartels L W and Lagendijk J J W 2007 7 T body MRI: B_1 shimming with simultaneous SAR reduction *Phys. Med. Biol.* **52** 5429–41

Vaughan J T *et al* 2001 7 T versus 4 T: RF power, homogeneity, and signal-to-noise comparison in head images *Magn. Reson. Med.* **46** 24–30

Yarnykh V L 2007 Actual flip-angle imaging in the pulsed steady state: a method for rapid three-dimensional mapping of the transmitted radiofrequency field *Magn. Reson. Med.* **57** 192–200